Inorganic Chemistry

Article

pubs.acs.org/IC

Structural and Electronic Comparison of 1st Row Transition Metal Complexes of a Tripodal Iminopyridine Ligand

Ashley M. McDaniel, Anthony K. Rappé, and Matthew P. Shores*

Department of Chemistry, Colorado State University, Fort Collins Colorado 80523-1872, United States

Supporting Information

ABSTRACT: We report the preparation and characterization of a series of divalent 3d transition metal complexes (Cr to Zn, **1**−**7**), featuring the multidentate, tripodal iminopyridine Schiff-base ligand trimethyl 6,6′,6″-((1E,1′E,1″E)-((nitrilotris(ethane-2,1-diyl))tris(azanylylidene))tris-(methanylylidene))-trinicotinate ($L^{5\text{-OOMe}}$). X-ray structural studies carried out on **1**−**5** and **7** reveal complex geometries ranging from local octahedral coordination to significant distortion toward trigonal prismatic geometry to heptacoordinate environments. Regardless of coordination mode, magnetic and spectroscopic studies show the ligand to provide moderately strong ligand fields: the Fe complex is low-spin, while the Co and Mn complexes are high-spin at all temperatures probed. Cyclic voltammograms exhibit multiple reversible ligand-based reductions, which are relatively consistent throughout the series; however, the electrochemical behavior of the Cr complex **1** is fundamentally different from those of the other complexes. Time-dependent (TD) density functional theory (DFT) and natural transition orbital (NTO) computational analyses are presented for the ligand, its anion, and complexes **1**−**7**: the computed spectra reproduce the major differential features of the observed visible absorption spectra, and NTOs provide viable interpretations for the observed features. The combined studies indicate that all complexes contain neutral ligands bound to M(II) ions, except for the Cr complex **1**, which is best described as a Cr(III) species bound to a radical anionic ligand.

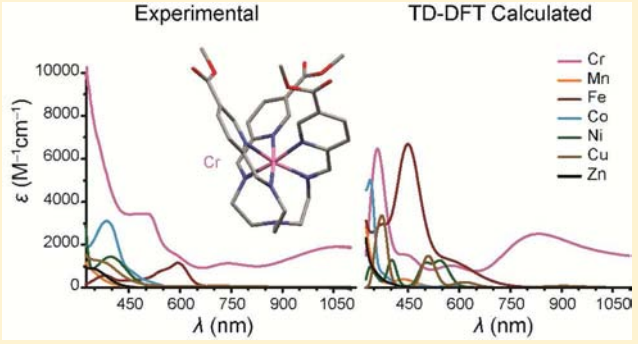

INTRODUCTION

Iminopyridine ligands generate interesting chemistry when bound to a wide variety of metal ions. These types of ligands can engender unique magnetic properties, such as frameworks that support spin-crossover with Fe(II),[1−3] and can promote unusual and novel reactivity in other first row transition metals. Complexes with iminopyridine ligands have been studied as polymerization catalysts,[4−6] dinitrogen activators,[7] water reduction catalysts,[8] and reservoirs for electrons (i.e., non-innocent ligands).[9]

We are particularly interested in tripodal iminopyridine ligands (Scheme 1) that may support novel magnetic and/or electronic properties in first-row transition metal complexes. In principle, such a multidentate ligand set should improve solution stability, provide steric and electronic tunability, and offer coordination modes for anisotropic interfacing of the complex with its environment. To illustrate, efforts to demonstrate anion-dependent spin-state switching or solar-photoconversion require that substitutionally labile species (e.g., high-spin Fe(II), Cr(II), excited states of Cr(III)) be corralled in solution.[10,11]

More specifically, the coordination environments and chemical properties of tren-based tripodal iminopyridine ligands have been a subject of previous studies.[1,12−16] These scaffolds have seven potential metal-binding sites for chelation, are flexible enough to support different coordination modes depending on the metal center, and tend to be amenable to modular synthetic schemes. Minor alterations in ligand functionalization can produce substantial changes in the coordination environment of the chelated metal. The ability of the tripodal ligand to twist about the M−N_{tether} 3-fold axis can give rise to coordination modes ranging from trigonal antiprismatic (locally octahedral) to trigonal prismatic geo-

Scheme 1. Left: Generalized Example of an Iminopyridine Ligand.[a] Right: Tripodal Ligand $L^{5\text{-OOMe}}$ Studied in This Work

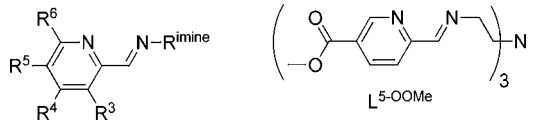

[a]Functionalization at R^5 can be used to attach the ligand to substrates. Functionalization at R^6 can be used to favor high-spin states in Fe(II) complexes. Alteration of R^{imine} can affect coordination geometry.

Received: August 31, 2012
Published: November 8, 2012

metries. Previously reported tren-based tripodal iminopyridine complexes tend toward trigonal antiprismatic geometries.[12]

Along with variation in the trigonal twist angle, functional groups appended to the pyridine moiety can alter metal coordination environment. The steric bulk of groups at the 6-position hinders close approach of the pyridine N to the metal center, causing the M−N bonds to lengthen as compared to the unfunctionalized complexes. This is of particular importance in the case of Fe(II), where longer M−N bonds favor the high-spin state over the low-spin state.[17−21] Structural variations of this nature can lead to dramatic changes in the compounds' physical, chemical, and magnetic properties.[18,22]

One avenue of potential property perturbation that has not been widely explored is the modification of ligand electronics by addition of functional groups that do not sterically interact with the bound metal center. Focusing on iminopyridine-type ligands,[23] aside from methyl incorporation at various points on the pyridine,[12] the only other type of functionalization that has been explored for tren-based iminopyridine ligands has been inclusion of long chain alkyl groups at the 5-position to produce metallomesogens.[24,25] These types of functionalizations typically alter the way molecules pack, but do not seem to impart significant effects on the complexes' electronics.

In this work, we probe how incorporation of an electron-withdrawing substituent on a tren-based iminopyridine ligand affects the structural and electronic properties of divalent metal complexes. The impetus for this research is to tune complex electronic structure for possible exploitation in solar photoconversion (Cr, Zn) and spin-crossover (Cr, Mn, Fe, Co) applications. In addition, changes in ion size and d electron count across the first transition series may reasonably be expected to offer several coordination modes, highlighting the ligand's structural flexibility. To study how electronic alterations to the ligand affect properties, we selected an ester functionalization at the 5-position of the pyridine. The ester acts as an electron withdrawing group and can significantly affect the electronics of the ligand and its resulting complexes in $[Cr(polypyridine)_3]^{3+}$ analogues.[11] In addition to its electron withdrawing properties, the ester group provides (a) precursors for anchoring complexes to semiconductor substrates,[26] directly related to our ongoing studies in solar photoconversion;[11] and (b) convenient entry points to access other types of functionalization, including potential anion binding sites, which may be used to influence spin-crossover in solution and in the solid state.[10,27]

Here, we present a comparison of the properties of new $[M(\mathbf{L}^{5\text{-OOMe}})]^{2+}$ complexes, where $\mathbf{L}^{5\text{-OOMe}}$ is trimethyl 6,6′,6″-((1E,1′E,1″E)-((nitrilotris(ethane-2,1-diyl))tris-(azanylylidene))tris-(methanylylidene))trinicotinate, and M = Cr, Mn, Fe, Co, Ni, Cu, Zn. We observe coordination flexibility throughout the 3d series as well as interesting behavior in the $[Cr(\mathbf{L}^{5\text{-OOMe}})]^{2+}$ complex, which differs significantly from the rest of the complexes studied.

EXPERIMENTAL SECTION

Preparation of Compounds. Unless otherwise noted, compound manipulations were performed either inside a dinitrogen-filled glovebox (MBRAUN Labmaster 130) or via Schlenk techniques on an inert gas (N_2) manifold. The preparations of dimethylpyridine-2,5-dicarboxylate,[28] methyl-6-(hydroxymethyl)nicotinate,[29] $[Cr(CH_3CN)_4(BF_4)_2]$,[30] and $Fe(CF_3SO_3)_2{\cdot}2CH_3CN$[31] have been described elsewhere. Methyl-6-formylnicotinate was synthesized according to a modified literature procedure,[32] where methyl-6-(hydroxymethyl)nicotinate was substituted as the oxidation substrate. Pentane was distilled over sodium metal and subjected to three freeze−pump−thaw cycles. Other solvents were sparged with dinitrogen, passed over molecular sieves, and degassed prior to use. All other reagents were obtained from commercial sources and were used without further purification.

Caution! *While we have not encountered any difficulties with compounds* **4** *and* **5** *at the scales described here, perchlorate-containing compounds pose an explosion hazard and should be handled with care and only in small quantities.*

Trimethyl 6,6′,6″-((1E,1′E,1″E)-((nitrilotris(ethane-2,1-diyl))-tris(azanylylidene))tris-(methanylylidene))trinicotinate ($\mathbf{L}^{5\text{-OOMe}}$). A solution of tren (0.05 g, 0.36 mmol) in 3 mL of anhydrous methanol was added to a solution of methyl-6-formylnicotinate (0.21 g, 1.25 mmol) in 5 mL of anhydrous methanol; the resulting solution was stirred at room temperature. Within 10 min, a white precipitate formed; the mixture was stirred for an additional 2 h. The solid was isolated by filtration, washed with anhydrous methanol (3 × 2 mL) and diethyl ether (3 × 2 mL) and dried in vacuo to afford 0.17 g (79%) of product. ^{1}H NMR ($CDCl_3$): 3.00 (6H, t), 3.80 (6H, t), 3.97 (9H, s) 7.97 (3H, d), 8.27 (3H, dd). 8.35 (3H, s), 9.16 ppm (3H, d). ^{13}C NMR ($CDCl_3$): 52.71, 55.29, 60.18, 120.84, 126.64, 137.77, 150.81, 157.80, 162.26, 165.67 ppm. IR (KBr pellet): $\nu_{C=O}$ 1723, $\nu_{C=N}$ 1646 cm^{-1}. Absorption spectrum (CH_3CN): λ_{max} 203, 245, 256 (sh), 279 nm. HRES+MS (CH_3OH): m/z 588.2580 ($\mathbf{L}^{5\text{-OOMe}}$+H)$^+$, 610.2395 ($\mathbf{L}^{5\text{-OOMe}}$+Na)$^+$.

$[Cr(\mathbf{L}^{5\text{-OOMe}})](BF_4)_2$ (1). A solution of $[Cr(MeCN)_4(BF_4)_2]$ (0.132 g, 0.340 mmol)) in 5 mL of acetonitrile was added to a suspension of $\mathbf{L}^{5\text{-OOMe}}$ (0.200 g, 0.340 mmol) in 8 mL of acetonitrile. The resulting dark brown solution was stirred at room temperature for 16 h. After concentrating the solvent in vacuo to ∼2 mL, the addition of 20 mL of diethyl ether produced a dark brown precipitate. The powder was collected by filtration, washed with diethyl ether (3 × 4 mL) and pentane (3 × 2 mL), and dried in vacuo to afford 0.225 g (81%) of product. IR (KBr pellet): $\nu_{C=O}$ 1733, $\nu_{C=N}$ 1603 cm^{-1}. Absorption spectrum (MeCN): λ_{max} (ε_M) 199 (53000), 228 (31000, sh), 290 (20000), 478 (3500), 586 (1600, sh), 738 (1200), 1068 nm (1900 M^{-1}cm^{-1}). μ_{eff} (295 K): 3.40 μ_B. μ_{eff} (5 K): 2.83 μ_B. ES+MS (MeCN): m/z 319.73 ($[Cr(\mathbf{L}^{5\text{-OOMe}})]^{2+}$). Anal. calcd. for $C_{30}H_{33}B_2CrF_8N_7O_6$: C, 44.31; H, 4.09; N, 12.06. Found: C, 44.22; H, 4.38; N, 12.35. Crystals of $\mathbf{1}{\cdot}CH_3OH$ suitable for X-ray analysis were obtained by slow diffusion of diethyl ether into a methanolic solution of the compound.

$[Mn(\mathbf{L}^{5\text{-OOMe}})](CF_3SO_3)_2$ (2). A solution of $Mn(CF_3SO_3)_2$ (0.06 g, 0.17 mmol) in 3 mL of methanol was added to a suspension of $\mathbf{L}^{5\text{-OOMe}}$ (0.10 g, 0.17 mmol) in 5 mL of methanol. The resulting light yellow solution was stirred at room temperature for 16 h. After concentrating the solvent in vacuo to ∼2 mL, the addition of 20 mL of diethyl ether produced a yellow precipitate. The powder was collected by filtration, washed with diethyl ether (3 × 2 mL), and dried in vacuo to afford 0.143 g (89%) of product. IR (KBr pellet): $\nu_{C=O}$ 1733, $\nu_{C=N}$ 1601 cm^{-1}. Absorption spectrum (MeCN): λ_{max} (ε_M) 195 (58000), 239 (35000), 280 (26000, sh), 287 (31000), 297 (25000, sh), 342 nm (850 M^{-1}cm^{-1}). μ_{eff} (295 K): 6.46 μ_B. μ_{eff} (5 K): 6.01 μ_B. ES+MS (MeCN): m/z 791.20 ($[Mn(\mathbf{L}^{5\text{-OOMe}})(CF_3SO_3)]^+$). Anal. calcd. for $C_{32}H_{33}F_6MnN_7O_{12}S_2$: C, 40.86; H, 3.54; N, 10.42. Found: C, 40.72; H, 3.26; N, 10.42. Crystals of **2** suitable for X-ray analysis were obtained by slow diffusion of diethyl ether into an acetonitrile solution of the compound.

$[Fe(\mathbf{L}^{5\text{-OOMe}})](CF_3SO_3)_2$ (3). A solution of $Fe(CF_3SO_3)_2{\cdot}2CH_3CN$ (0.045 g, 0.102 mmol) in 3 mL of acetonitrile was added to a suspension of $\mathbf{L}^{5\text{-OOMe}}$ (0.060 g, 0.102 mmol) in 5 mL of acetonitrile. The resulting dark purple solution was stirred for 16 h. After concentrating the solvent in vacuo to ∼2 mL, the addition of 20 mL of diethyl ether produced a purple-black precipitate. The powder was collected by filtration, washed with diethyl ether (3 × 2 mL) and pentane (3 × 2 mL), and dried in vacuo to afford 0.082 g (85%) of product. IR (KBr pellet): $\nu_{C=O}$ 1731, $\nu_{C=N}$ 1601 cm^{-1}. Absorption spectrum (MeCN): λ_{max} (ε_M) 200 (66000), 239 (26000), 281 (40000), 289 (36000, sh), 382 (570), 540 (760, sh), 594 nm (1160 M^{-1}cm^{-1}). ^{1}H NMR (CD_3CN): 9.67 (br s, 3H); 8.66 (dd, 3H); 8.48 (dd, 3H); 7.74 (br s, 3H); 3.96 (br m, 6H); 3.81 (s, 9H); 3.19 (m,

dx.doi.org/10.1021/ic301909u | Inorg. Chem. 2012, 51, 12493−12502

Table 1. Crystallographic Data[a] for Compounds 1−5 and 7

	1·CH_3OH	2	3	4a	5·2CH_3CN	7
formula	$C_{31}H_{37}B_2CrF_8N_7O_7$	$C_{32}H_{33}F_6MnN_7O_{12}S_2$	$C_{32}H_{33}F_6FeN_7O_{12}S_2$	$C_{30}H_{33}Cl_4Co_2N_7O_6$	$C_{34}H_{39}Cl_2N_9NiO_{14}$	$C_{32}H_{33}F_6N_7O_{12}S_2Zn$
fw	845.30	940.71	941.62	847.29	927.35	951.14
color, habit	brown needles	yellow plates	purple plates	green plates	orange plates	yellow blocks
T, K	120(2)	120(2)	120(2)	120(2)	120(2)	120(2)
space group	$P\bar{1}$	$P\bar{1}$	$P2_1c$	$P2_13$	$P\bar{1}$	$R3$
Z	2	2	4	4	2	3
a, Å	11.8630(4)	12.5586(11)	15.6283(13)	15.4332(4)	12.3690(8)	10.042(2)
b, Å	12.9273(5)	12.6047(11)	19.4132(16)	15.4332(4)	12.7685(8)	10.042(2)
c, Å	13.1753(5)	12.8933(11)	14.4401(13)	15.4332(4)	13.9210(9)	35.268(9)
α, deg	81.305(2)	93.705(5)	90	90	73.345(3)	90
β, deg	71.683(2)	94.262(5)	115.895(4)	90	86.927(3)	90
γ, deg	71.499(2	103.718(5)	90	90	73.045(3)	120
V, Å^3	1816.04(12)	1970.1(3)	3941.2(6)	3675.94(17)	2013.7(2)	3079.8(12)
d_{calc}, g/cm^3	1.546	1.586	1.587	1.531	1.529	1.538
GOF	1.028	1.042	1.016	1.036	1.034	1.068
$R_1(wR_2)^b$, %	5.05 (12.81)	4.34 (11.60)	4.04 (10.53)	2.31 (5.56)	3.70 (10.24)	4.23 (12.47)

[a]Obtained with graphite-monochromated Mo Kα (λ = 0.71073 Å) radiation. [b]$R_1 = \sum||F_o| - |F_c||/\sum|F_o|$, $wR_2 = \sum[w(F_o^2 - F_c^2)^2]/\sum[w(F_o^2)^2]\}^{1/2}$ for $F_o > 4\sigma(F_o)$.

6H). μ_{eff} (295 K): 0.94 μ_B. ES+MS (MeCN): m/z 792.13 ([Fe($L^{5\text{-OOMe}}$)(CF_3SO_3)]$^+$), 321.73 ([Fe($L^{5\text{-OOMe}}$)]$^{2+}$). Anal. calcd. for $C_{32}H_{33}F_6FeN_7O_{12}S_2$: C, 40.82; H, 3.53; N, 10.41. Found: C, 40.58; H, 3.25; N, 10.47. Crystals of **3**·0.62Et_2O suitable for X-ray analysis were obtained by slow diffusion of diethyl ether into an acetonitrile solution of the compound.

[Co($L^{5\text{-OOMe}}$)](ClO_4)$_2$ (4). A solution of Co(ClO_4)$_2$·6H_2O (0.044 g, 0.119 mmol) in 3 mL of methanol was added to a stirring suspension of $L^{5\text{-OOMe}}$ (0.070 g, 0.119 mmol) in 5 mL of methanol. Within 10 min, an orange precipitate formed; the mixture was stirred for 16 h. The solid was collected by filtration, washed with methanol (3 × 3 mL) and diethyl ether (3 × 2 mL), and dried in vacuo to afford 0.091 g (91%) of product. IR (KBr pellet): $\nu_{C=O}$ 1719, $\nu_{C=N}$ 1603 cm^{-1}. Absorption spectrum (MeCN): λ_{max} (ε_M) 194 (61400), 239 (33000), 285 (29200), 385 nm (3100 M^{-1}cm^{-1}). μ_{eff} (295 K): 4.38 μ_B. μ_{eff} (5 K): 4.15 μ_B. ES+MS (MeCN): m/z 745.13 ([Co($L^{5\text{-OOMe}}$)(ClO_4)]$^+$). Anal. calcd. for $C_{30}H_{33}Cl_2CoN_7O_{14}$: C, 42.62; H, 3.93; N, 11.60. Found: C, 42.66; H, 3.98; N, 11.49. Crystalline material can be obtained by slow diffusion of diethyl ether into an acetonitrile solution of the compound, but the crystals were not suitable for X-ray analysis.

[Co($L^{5\text{-OOMe}}$)][$CoCl_4$] (4a). A solution of $CoCl_2$ (0.021 g, 0.17 mmol) in 3 mL of methanol was added to a stirring suspension of $L^{5\text{-OOMe}}$ (0.100 g, 0.17 mmol) in 5 mL of methanol. Initially an orange solution formed; it was stirred for an additional 16 h, whereupon the color slowly turned brown-green. A brown-green power was precipitated by addition of diethyl ether. The solid was collected by filtration, washed with diethyl ether (3 × 2 mL), and recrystallized by diethyl ether diffusion into methanol to yield green crystals of the product. IR (KBr pellet): $\nu_{C=O}$ 1727, $\nu_{C=N}$ 1600 cm^{-1}. Absorption spectrum (MeCN): λ_{max} 194, 239, 285, 385, 616 nm. ES+MS (MeCN): m/z 681.07 ([Co($L^{5\text{-OOMe}}$)(Cl)]$^+$), 323.13 ([Co($L^{5\text{-OOMe}}$)]$^{2+}$).

[Ni($L^{5\text{-OOMe}}$)](ClO_4)$_2$ (5). A solution of Ni(ClO_4)$_2$·6H_2O (0.065 g, 0.177 mmol) in 3 mL of methanol was added to a stirring suspension of $L^{5\text{-OOMe}}$ (0.105 g, 0.177 mmol) in 5 mL of methanol. In the first 10 min, an orange precipitate forms, and the mixture is allowed to stir for 16 h. The solid was collected by filtration, washed with methanol (3 × 3 mL) and diethyl ether (3 × 2 mL), and dried in vacuo to afford 0.13 g (87%) of product. IR (KBr pellet): $\nu_{C=O}$ 1723, $\nu_{C=N}$ 1604 cm^{-1}. Absorption spectrum (MeCN): λ_{max} (ε_M) 199 (65000), 239 (33000), 284 (28000), 396 (1500), 866 nm (9.8 M^{-1}cm^{-1}). μ_{eff} (295K): 3.44 μ_B. ES+MS (MeCN): m/z 744.20 ([Ni($L^{5\text{-OOMe}}$)(ClO_4)]$^+$), 322.73 ([Ni($L^{5\text{-OOMe}}$)]$^{2+}$). Anal. calcd. for $C_{30}H_{33}Cl_2N_7NiO_{14}$: C, 42.63; H, 3.94; N, 11.60. Found: C, 42.45; H, 3.83; N, 12.03. Crystals of **5**·2CH_3CN suitable for X-ray analysis were obtained by slow diffusion of diethyl ether into an acetonitrile solution of the compound.

[Cu($L^{5\text{-OOMe}}$)](CF_3SO_3)$_2$ (6). A solution of Cu(CF_3SO_3)$_2$ (0.065 g, 0.18 mmol) in 3 mL of acetonitrile was added to a stirring suspension of $L^{5\text{-OOMe}}$ (0.106 g, 0.18 mmol) in 5 mL of acetonitrile. The resulting mossy green solution was stirred for two hours and then was concentrated in vacuo to ~2 mL. Mossy green crystals were obtained from slow diffusion of diethyl ether into the concentrated acetonitrile solution, and were collected by filtration. The collected crystals were washed with diethyl ether (3 × 2 mL) and pentane (3 × 2 mL) to afford 0.129 g (75%) of product. IR (KBr pellet): $\nu_{C=O}$ 1728, $\nu_{C=N}$ 1606 cm^{-1}. Absorption spectrum (MeCN): λ_{max} (ε_M) 195 (55000), 236 (38000), 286 (28000), 295 (25000, sh), 353 (1300, sh), 713 nm (85 M^{-1}cm^{-1}). μ_{eff} (295 K): 2.27 μ_B. μ_{eff} (5 K): 1.80 μ_B ES+MS (MeCN): m/z 799.07 ([Cu($L^{5\text{-OOMe}}$)(CF_3SO_3)]$^+$). Anal. calcd. for $C_{32}H_{33}CuF_6N_7O_{12}S_2$: C, 40.49; H, 3.50; N, 10.33. Found: C, 40.66; H, 3.70; N, 10.64. Crystalline samples of **6** can be obtained by slow diffusion of diethyl ether into methanol or acetonitrile; the crystals tend to be very large but very thin sheets/needles, and thus far have not been suitable for X-ray analysis.

[Zn($L^{5\text{-OOMe}}$)](CF_3SO_3)$_2$ (7). A solution of Zn(CF_3SO_3)$_2$ (0.123 g, 0.34 mmol) in 4 mL of methanol was added to a stirring suspension of $L^{5\text{-OOMe}}$ (0.200 g, 0.34 mmol) in 3 mL of acetonitrile. The resulting yellow solution was stirred for two hours, and then was concentrated in vacuo to ~2 mL. Crystals were obtained from slow diffusion of diethyl ether into the concentrated methanol solution and were collected by filtration. The collected crystals were washed with diethyl ether (3 × 2 mL) and pentane (3 × 2 mL) to afford 0.276 g (85%) of product. IR (KBr pellet): $\nu_{C=O}$ 1726, $\nu_{C=N}$ 1601 cm^{-1}. Absorption spectrum (MeCN): λ_{max} (ε_M) 195 (59000), 240 (39000), 287 (32000), 294 (26000, sh), 340 nm (910 M^{-1}cm^{-1}, sh). ^{1}H NMR (CD_3CN): 8.74 (s, 3H); 8.72 (dd, 3H); 8.13 (dd, 3H); 7.60 (d, 3H); 3.80 (s, 9H); 3.76 (m, 3H); 3.58 (dd, 3H); 3.23 (dd, 3H); 2.90 (td, 3H). ES+MS (MeCN): m/z 800.20 ([Zn($L^{5\text{-OOMe}}$)(CF_3SO_3)]$^+$), 325.67 ([Zn($L^{5\text{-OOMe}}$)]$^{2+}$. Anal. calcd. for $C_{32}H_{33}F_6N_7O_{12}S_2Zn$: C, 40.41; H, 3.50; N, 10.31;. Found: C, 40.37; H, 3.29; N, 10.15. Crystals of 7 suitable for X-ray analysis were obtained by slow diffusion of diethyl ether into an acetonitrile solution of the compound.

X-ray Structure Determinations. Crystals suitable for X-ray analysis were coated with Paratone-N oil and supported on a Cryoloop before being mounted on a Bruker Kappa Apex II CCD diffractometer under a stream of dinitrogen. Data collection was performed at 120 K with Mo Kα radiation and a graphite monochromator, targeting complete coverage and 4-fold redundancy. Initial lattice parameters were determined from at least 270 reflections harvested from 36 frames; these parameters were later refined against all data. Crystallographic data and metric parameters are presented in Table 1. Data were integrated and corrected for Lorentz and polarization

dx.doi.org/10.1021/ic301909u | Inorg. Chem. 2012, 51, 12493−12502

Scheme 2. Syntheses of the Ligand $L^{5\text{-OOMe}}$ (top) and the Divalent Complex Salts 1−7 (bottom)

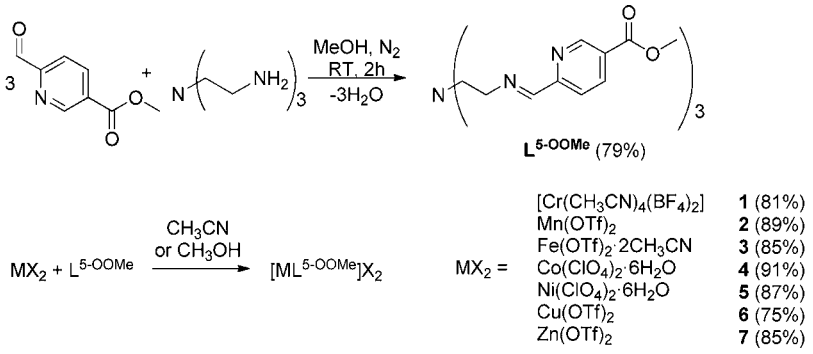

effects using SAINT, and semiempirical absorption corrections were applied using SADABS.[33] The structure was solved by direct methods and refined against F^2 with the SHELXTL 6.14 software package.[34] Unless otherwise noted, thermal parameters for all non-hydrogen atoms were refined anisotropically. Hydrogen atoms were added at the ideal positions and were refined using a riding model where the thermal parameters were set at 1.2 times those of the attached carbon atom (1.5 for methyl protons).

For the structure of **1**, both BF_4^- anions show significant disorder. The anion containing B1 is rotationally disordered over two positions (57:43 ratio) about the axis containing the B1-F1 bond. The anion containing F8 is disordered over two positions, where only F7 and F8 are common between the two. The major part (83%) contains B2a, F6a, and F5a, and the fluorine atoms in the major part were refined anisotropically. The major component of this anion was used to constrain the other BF_4^- bond distances and bond angles by the SAME command. All of the thermal parameters for the other disordered BF_4^- components were treated isotropically. A methanol solvate molecule was initially refined with partial site occupancy (84%) and was finally modeled with full occupation as this is more chemically reasonable; the thermal parameters were treated anisotropically.

In the structure of **2**, neither obvious disorder nor solvate molecules are observed; however, the highest residual peak is 2 $e^-/Å^3$, and the deepest hole is 0.97 $e^-/Å^3$. The residual electron density appears between S1 and C31 on one of the triflate anions, consistent with minor untreated triflate disorder.

In the structure of **3**, residual electron density in the trigonal "pocket" formed by the ester groups of the ligand cannot be modeled satisfactorily; they likely represent disordered and/or partially occupied molecules of diethyl ether (no $\nu_{C\equiv N}$ resonances are observed in the IR spectrum for crystals of **3**). This electron density was treated with SQUEEZE,[35] which finds a 144.8 $Å^3$ solvent void with 26 e^-/unit cell, corresponding to a partially occupied (62%) diethyl ether molecule. The data in Table 1 do not include the components removed by SQUEEZE.

For **4**, crystals of the perchlorate salt diffract well but have not produced reasonable structure solutions, possibly due to twinning. An alternative anion, $[CoCl_4]^{2-}$, produces a well-defined structure (**4a**) with no included solvent present and no disorder.

In the structure of **7**, the anions and cation reside on special positions with 3-fold symmetry. One of the triflate anions is disordered over two symmetry-related positions such that O and F atoms are located at the same position. This disorder was modeled simply as each site being occupied by a single type of atom (O or F) with half of the sites assigned to O and half assigned to F. Meanwhile, the triflate C−S axis does not coincide with the crystallographic 3-fold axis: this generates four sites over which the C and S are disordered. The disorder was modeled with two sites set as C and two set as S but no mixing of S and C positions.

Other Physical Methods. Absorption spectra were obtained with a Hewlett-Packard 8453 spectrophotometer in quartz cuvettes with 1 cm or 1 mm path lengths in air (or in an airfree glass cuvette under dinitrogen for **1**); all experiments were performed at room temperature. Infrared spectra were measured with a Nicolet 380 FT-IR spectrometer. Mass spectrometric measurements were performed in the positive ion mode on a Finnigan LCQ Duo mass spectrometer, equipped with an analytical electrospray ion source and a quadrupole ion trap mass analyzer. Cyclic voltammetry experiments were carried out inside a dinitrogen-filled glovebox in 0.1 M solutions of $(Bu_4N)PF_6$ in acetonitrile unless otherwise noted. The voltammograms were recorded with either a CH Instruments 1230A or 660C potentiostat, using a 0.25 mm Pt disk working electrode, Ag wire quasi-reference electrode, and a Pt wire auxiliary electrode. All voltammograms shown were measured with a scan rate of 0.1 V/s. Reported potentials are referenced to the ferrocenium/ferrocene ($Fc^{+/0}$) redox couple and were determined by adding ferrocene as an internal standard at the conclusion of each electrochemical experiment. Solid state magnetic susceptibility measurements were performed using a Quantum Design model MPMS-XL SQUID magnetometer at 295 and 5 K on finely ground samples prepared under a dinitrogen atmosphere. The data were corrected for the magnetization of the sample holder by subtracting the susceptibility of an empty container; diamagnetic corrections were applied using Pascal's constants.[36] ^{1}H NMR spectra were measured using Varian INOVA 300 or 400 MHz instruments. Magnetic susceptibilities in CD_3CN or d_6-DMSO solution were determined by the Evans method.[37−41] Elemental analyses were performed by Robertson Microlit Laboratories, Inc. in Madison, NJ.

Electronic Structure Calculations. Unrestricted B3LYP hybrid density functional SCF and TD-DFT studies[42] were carried out in the G09 suite of electronic structure codes.[43] The geometries for $[M(L^{5\text{-OOMe}})](BF_4)_2$ and $[Cr(L^{5\text{-OOMe}})](BF_4)_3$ were optimized as isolated, gas phase ion pairs; note that BF_4^- anions were used for all computed structures. Due to the importance of the amine nitrogen in the electronic spectroscopy, the $M-N_{amine}$ distance was constrained to the respective experimental distances shown in Figure S1. For Cu this distance optimized to 3.243 Å. The Cr cation and BF_4 anions were removed to generate the coordinates for $L^{5\text{-OOMe}}$. The LANL2 basis sets and effective core potentials were used for the transition metals;[44] H, B, C, N, O, and F were described with a 6-31g* model.[45−48] Simulated electronic absorption spectra utilized a Gaussian line shape, computed oscillator strengths and peak positions as well as a 0.15 eV line width.

RESULTS

Syntheses. Shown in Scheme 2, the ligand $L^{5\text{-OOMe}}$ is synthesized via Schiff base condensation of tren (tris-2(aminoethyl)amine) and a slight stoichiometric excess of methyl-6-formylnicotinate. The reaction product is a white precipitate and is isolated in good (79%) yield. The ligand is slightly soluble in polar organic solvents such as methanol, acetonitrile, chloroform, and dichloromethane, but it is insoluble in hydrocarbons and diethyl ether.

The preparations of the divalent metal complex salts are straightforward (Scheme 2). The complexes form upon mixing polar-organic solutions of MX_2 with slurries of the ligand in the

dx.doi.org/10.1021/ic301909u | Inorg. Chem. 2012, 51, 12493−12502

same solvent under an inert atmosphere. The choice of solvent is primarily dictated by the metal precursor: methanol was used for bare or hydrated metal salts, while acetonitrile was used for acetonitrile-solvated metal salts. The metalation reaction proceeds quickly as evidenced by almost immediate changes in the colors of the reaction mixtures. The tetrafluoroborate and triflate salts **1**−**3**, **6**, and **7** remain soluble but can be isolated by concentrating the reaction mixture, followed by precipitation with diethyl ether. The perchlorate salts **4** and **5** precipitate directly from solution and can be isolated by filtration. The isolated yields for the complexes are typically >80%. The product complexes are all generally air stable in the solid state and in solution; however, the Cr complex is air-sensitive in solution and must be handled under inert atmosphere. Crystalline material can be isolated by slowly diffusing diethyl ether into concentrated acetonitrile solutions of each of the complexes, although methanol gives better crystals for **1**. While Cr(II) complexes have been reported to disproportionate in protic solutions,[49] we observe no evidence of disproportionation of **1** in methanol.

Structural Comparisons. The X-ray structures determined for the compounds reported here (Table 1, Figure 1) reveal cationic mononuclear complexes that are in general well-separated from each other by charge balancing anions. All iminopyridine nitrogen atoms are bound to the metal ion; in the cases of the Mn and Co complexes **2** and **4**, the bridgehead (tren) nitrogen atom is significantly closer to the metal center (Figure 1 and, in the Supporting Information, Figure S1 and Table S1). The average trigonal twist angle φ[12] (Table S1) varies from 39.9° to 54.5°, which indicates that all of the complexes are closer in geometry to octahedral/trigonal antiprismatic rather than trigonal prismatic. The complexes most distorted away from octahedral local geometry contain Mn (**2**), Co (**4a**), and Zn (**7**) ions.

For this family of complexes, the metal nitrogen bonds follow a pattern where the M−N_{imine} bonds are shorter than the M−$N_{pyridine}$ bonds. In the more regularly octahedral complexes **1**, **3**, and **5**, this difference is small (~0.03 Å), while in the structures that are pronouncedly distorted from octahedral (**2**, **4a**, and **7**), the differences are much larger (0.15−0.25 Å). Chromium-containing **1** displays unusual variation between different arms of the tripodal ligand in addition to the metal-pyridine/imine bond variations. The Cr−N bonds on one of the ligand arms are shorter by at least 0.04 Å compared to the other two arms. This is accompanied by shortening of the C−C bond bridging between the two coordinating N atoms and lengthening of both N−C bonds (Table 2). These differences are consistent with radical anion character localized on the ligand arm interacting with a Cr(III) center; such bond alternation has been observed recently in other reduced forms of Cr diimine and iminopyridine compounds.[9,50]

In these complexes, the ester groups are part of the conjugated system including the pyridine and imine. Generally, the esters are nearly coplanar with the pyridines, and all complexes have ester-pyridine torsion angles of less than 20°. The Ni complex **5** has both the maximum (19.60°) and minimum (1.89°) torsion angles of all the complexes. It is interesting to note that, for every complex except Fe-containing **3**, the ester groups all point the same direction on all three arms, with the carbonyl oxygen pointing away from the metal center. However, in the Fe case, only one of the ester groups adopts this position. Additionally, the three ester groups can be thought to form a trigonal pocket. For complexes **1**, **3**, **4**, and **5**, the sides of the trigonal pocket[51] range from 5.3 to 6.5 Å. For complexes in **2** and **7**, the distances are much shorter and range

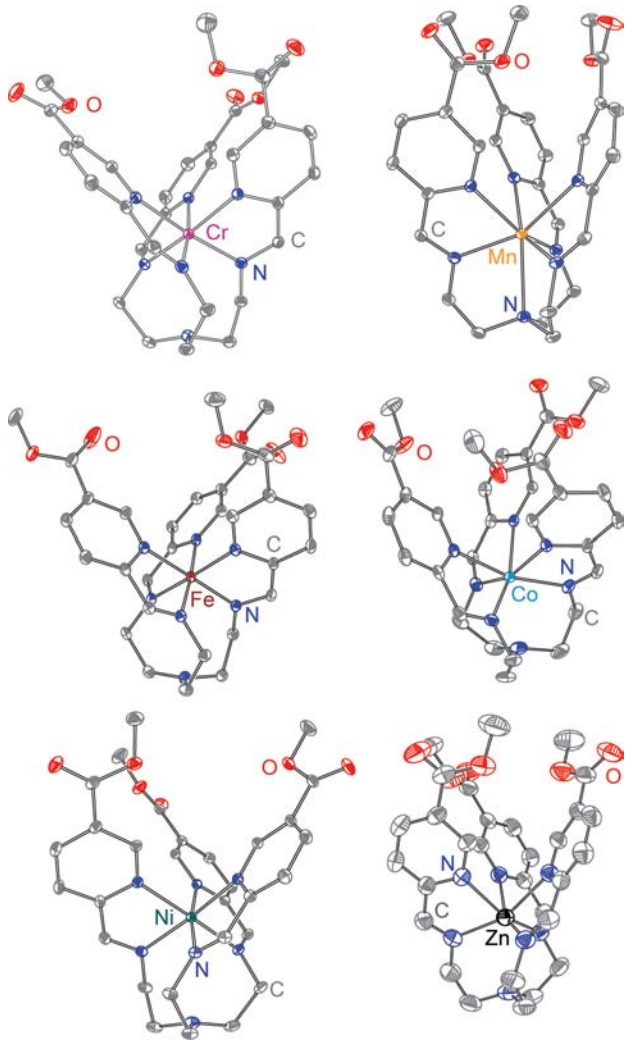

Figure 1. Side-on view of the $[M(L^{5\text{-OOMe}})]^{2+}$ complex cations in the structures of **1**−**5** and **7**, rendered with 40% probability ellipsoids. Pink, yellow, dark red, light blue, green, black, red, dark blue, and gray ellipsoids represent Cr, Mn, Fe, Co, Ni, Zn, O, N, and C atoms, respectively. All hydrogen atoms are omitted for clarity.

Table 2. Selected Iminopyridine Ligand Bond Lengths for 1 and Average Iminopyridine Ligand Bond Lengths for Complexes 2−5, 7, and $[Cr(L^{5\text{-OOMe}})](BF_4)_3$

complex (metal)	*x* (Å)	*y* (Å)	*z* (Å)
1 (Cr)	1.361(3)	1.454(3)	1.288(3)
	1.365(2)	1.465(3)	1.280(3)
	1.376(3)	**1.420(3)**	**1.311(3)**
2 (Mn)	1.352 [3][a]	1.474[3][a]	1.271[3][a]
3 (Fe)	1.362[3][a]	1.451[3][a]	1.287[3][a]
4 (Co)	1.351(1)[b]	1.469(2)[b]	1.267(2)[b]
5 (Ni)	1.353[2][a]	1.468[2][a]	1.274[2][a]
7 (Zn)	1.350(5)[b]	1.468(5)[b]	1.255(6)[b]
$[Cr(L^{5\text{-OOMe}})](BF_4)_3$[c]	1.364(2)[b]	1.463(2)[b]	1.275(2)[b]

[a]The errors for these bond distances were calculated by averaging the bond distances for each type of bond and taking the square root of the sum of the squares of the bond esds. [b]There is only one crystallographically independent bond of this type, so there are no average bond distances. [c]See ref 58.

dx.doi.org/10.1021/ic301909u | *Inorg. Chem.* 2012, 51, 12493−12502

from 3.9 to 4.6 Å. The smaller trigonal pocket coincides with the much smaller twist angles for these two complexes, and distortion away from octahedral geometry.

Comparison of Magnetic Properties. The room temperature magnetic moments for **1**−**6** indicate that compounds **2**, **4**, and **5** contain high-spin ions with 5, 3, and 2 unpaired electrons, respectively. Meanwhile, the data for **1** and **3** are consistent with low-spin Cr(II) and Fe(II) ions, containing 2 and 0 unpaired electrons, respectively. Note that for **1** the magnetic data is equally consistent with strong antiferromagnetic coupling between a ligand radical anion and a Cr(III) cation to give an $S = 1$ ground spin state, and such coupling has been previously observed for $[Cr^{III}(bpy)_2(bpy^{\bullet-})]^{2+}$-type complexes.[50] In addition to the solid state magnetic moment measurements, solution susceptibility measurements carried out on **3** show that the Fe(II) ion remains low spin and diamagnetic up to 80 °C in d_6-DMSO. For Ni(II) and Cu(II), single electron configurations with two and one unpaired electrons, respectively, are expected, and these are observed for compounds **5** and **6**. A solid state magnetic moment was not collected for complex **7** due to the d^{10} configuration for Zn(II); diamagnetism in solution is confirmed by Evans' method (^{1}H NMR) susceptibility measurements. Magnetic moments of **1**, **2**, and **4** collected at 5 K indicate that the low temperature spin states are unchanged from the room temperature determinations.

Electronic Absorption Comparisons. The ground state UV−visible absorption properties of each of the complexes were studied in acetonitrile solution at room temperature. Shown in Figure S2, each of the complexes shows three intense absorption bands in the ultraviolet part of the spectrum, with molar absorptivities greater than 25000 $M^{-1}\cdot cm^{-1}$. These bands are analogous to three UV bands present for the free ligand but are shifted slightly: the band at 245 nm in the free ligand is blue-shifted to 239 nm in each of the complexes, and the lowest energy UV band at 279 nm in the free ligand is red-shifted by 5−8 nm in the complexes.

The visible absorption spectra for **1**−**7** are shown in Figure 2 (top). The high-spin complexes (**2**, **4**, and **5**) and complexes **6** and **7** are all similar and devoid of strong features at wavelengths longer than 500 nm. Complex **2** has no absorption bands in the visible region, while complexes **4** and **7** have a band of moderate intensity centered at 386 and 340 nm, respectively. The Ni complex **5** has a moderately intense band centered at 395 nm and a very weak band at 866 nm; the latter is indicative of a d−d transition. The Ni(II) d−d band at 866 nm can be used to calculate Δ_o, the energy difference between the t_{2g} and e_g orbitals in this approximately octahedral ligand field. For **5**, Δ_o corresponds to 11550 cm^{-1}. Complex **6** displays similar features to **5**, with a moderately intense band at 353 nm and a weak band at 713 nm. The low-spin complex **3** has a rich visible absorption spectrum compared to the previously discussed species: the Fe complex displays bands of moderate intensity at 382, 540, and 594 nm.

The Cr compound **1** exhibits moderately intense absorption throughout the visible and into the near IR, with prominent peaks at 478, 586, 738, and 1068 nm. This behavior is qualitatively different from the other divalent metal complexes reported here. We note that transitions through the visible and into the near IR of similar band intensity are observed for Cr(III) complexes chelated to anionic bipyridine ligand radicals.[50]

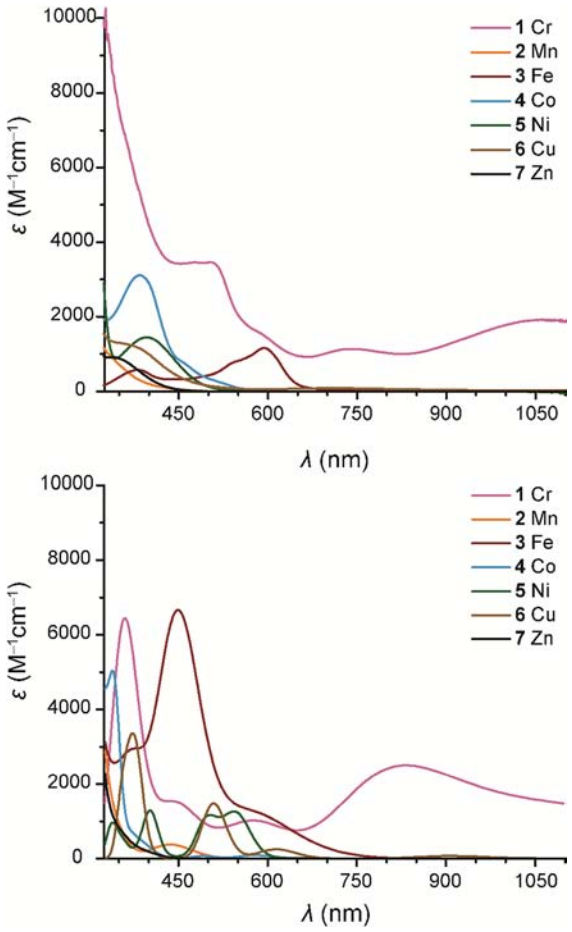

Figure 2. Experimental (top) and TD-DFT simulated (bottom) visible electronic absorption spectra for **1**−**7**, plotted on the same relative scales. Experimental data were collected on solutions in acetonitrile.

Simulated Electronic Absorption Spectra. To understand the observed periodic trends in the visible absorption spectra, TD-DFT and natural transition orbital (NTO) analyses have been carried out on the free $L^{5\text{-}OOMe}$ ligand and its anion (Figure S3, Supporting Information) and complexes **1**−**7** (Figures 2 and S4 (Supporting Information)). In general, simulated peaks are composed of more than one transition; representative NTO pairs are associated with the relevant transitions (Figure S4, Supporting Information) to highlight the orbital character of the peaks.

For the free ligand $L^{5\text{-}OOMe}$, at the computed geometry for **1**, the lowest energy transitions (λ < 550 nm) correspond to transitions from the bridgehead nitrogen lone pair → iminopyridine π^* orbitals. The HOMO of trimethylamine is provided in Figure S5 to illustrate the orbital character of a typical amine lone pair. When the free ligand is reduced, the bridgehead nitrogen lone pair transitions shift to lower wavelength and new iminopyridine → iminopyridine π^* bands appear at 600 and 900 nm.

The experimental and computed complex visible spectra collected in Figure 2 at the same scale suggest that the computed spectra reproduce the major differential features of the observed visible spectra. Specifically, **1** displays a number of high wavelength (λ > 500 nm) features. The Fe(II) complex **3** has a significant transition around 600 nm. The Mn(II), Co(II), and Zn(II) transitions in **2**, **4**, and **7**, respectively, are weaker and tend toward lower wavelengths, while the computed Ni(II)

and Cu(II) spectra (**5** and **6**) display high wavelength features not present in the observed spectra.

Select NTOs collected in Figure S4b–h (Supporting Information) provide viable interpretations for the observed features. For the computed spectrum of **1** provided in Figure 2 (bottom), a number of low intensity transitions contribute to the broad band above 550 nm: they correspond to iminopyridine → iminopyridine π^* bands (Figure S4b, Supporting Information), comparable to those computed for the anion of $\mathbf{L}^{5\text{-OOMe}}$ discussed above (Figure S3, Supporting Information). Bridgehead nitrogen lone pair → iminopyridine π^* transitions are computed to occur around 450 nm, and transitions with significant $t_{2g} \rightarrow e_g^*$ character are found below 400 nm. For **2** (Figure S4c, Supporting Information), low intensity bridgehead nitrogen lone pair → iminopyridine π^* transitions are computed near 450 nm and iminopyridine → iminopyridine π^* bands below 400 nm. As expected for low spin **3** (Figure S4d, Supporting Information), there is significant metal d orbital participation in the prominent 400–450 nm features correspond to a metal (t_{2g}) → iminopyridine π^* transitions, while the weaker (λ > 600 nm) transitions represent bridgehead nitrogen lone pair → iminopyridine π^* character. For the Co(II) complex **4** (Figure S4e, Supporting Information) the highest wavelength transitions display bridgehead nitrogen lone pair → iminopyridine π^* character. For the Ni(II) complex **5** (Figure S4f, Supporting Information), the highest wavelength transition possesses significant metal $t_{2g} \rightarrow e_g^*$ character; bridgehead nitrogen lone pair → iminopyridine π^* transitions occurring at lower wavelength. For the Cu(II) complex **6** (Figure S4g, Supporting Information) a high wavelength bridgehead nitrogen lone pair → e_g^* transition is inserted into the spectrum. When Zn(II) is inserted into the ligand to make **7** (Figure S4h, Supporting Information) the bridgehead nitrogen lone pair → iminopyridine π^* transition shifts to lower wavelength (λ < 450 nm), relative to the free ligand.

Electrochemistry. Each of the complexes displays rich electrochemical behavior (Figure 3). The hallmark of these species is the presence of multiple reversible reductions. For **2**–**5** and **7**, three reversible reductions between −1.0 and −1.75 V (vs $Fc^{0/+}$) and one irreversible reduction at potentials more negative than −2.10 V are observed. For each of the complexes, an irreversible oxidation is observed at positive potentials greater than 1.0 V. The electrochemical events common to all complexes are most likely ligand-based, since they vary little with the identity of the chelated metal. Additionally, the participation of other iminopyridine ligands in redox behavior has been previously observed for divalent first row transition-metal complexes.[9]

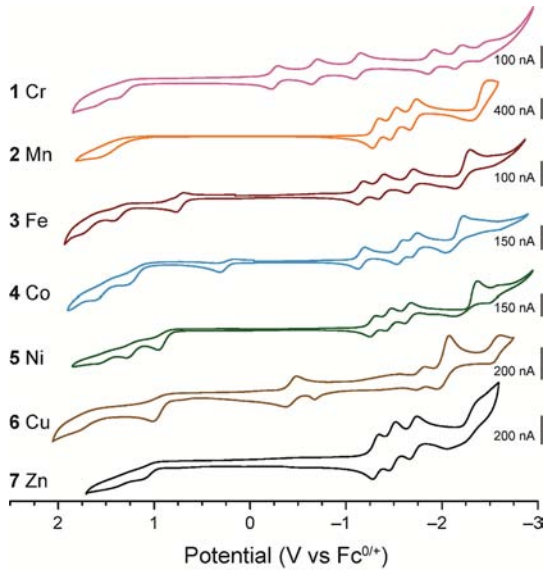

Figure 3. Cyclic voltammograms of the M(II) complexes in **1**–**7**, collected in 0.1 M $TBAPF_6$ acetonitrile solution with a scan rate of 100 mV/s. The potentials are referenced to ferrocene.

In addition to the redox events described, involvement of the metal ion is also evident for **3**–**6**. Compounds **3** and **4** also display one reversible oxidation at +0.71 and +0.26 V, respectively, which are tentatively assigned to metal-based 2+/3+ couples. The very positive potential for oxidation of the Fe complex falls between reported potentials assigned to the $Fe^{3+/2+}$ couple for similar $[Fe(iminopyridine)_3]^{2+}$ complexes.[52,53] The assigned $Co^{3+/2+}$ couple for **4** also matches closely to the potential reported for a similar $[Co(iminopyridine)_3]^{2+}$ complex.[53] The Ni complex **5** exhibits an additional quasi-reversible reduction at −2.51 V, tentatively assigned to the $Ni^{2+/1+}$ couple, which occurs at slightly more negative potentials than those reported for hexacoordinate iminopyridine Ni(II) complexes.[54,55] An irreversible oxidation occurs at +1.04 V and is tentatively assigned to the oxidation of Ni(II) to Ni(III). The Cu complex **6** displays an additional reversible reduction at −0.43 V, which is assigned to the 2+/1+ couple. This falls between the reported oxidation potentials for a di-Cu(I) iminopyridine cryptand and the reduction potentials of its di-Cu(II) aminopyridine cryptand analogue, which are each assigned to the Cu 2+/1+ couple.[56,57]

The behavior for the Cr complex **1** is qualitatively different than that of the other metal complexes. For **1**, four reversible reductions, one quasi-reversible reduction right at the edge of the solvent window, and one reversible oxidation are observed. The $E_{1/2}$ potentials for the events in **1** are essentially identical to those found for the trivalent analogue, $[Cr(\mathbf{L}^{5\text{-OOMe}})](BF_4)_3$.[58] However, the rest potentials for **1** and for $[Cr(\mathbf{L}^{5\text{-OOMe}})](BF_4)_3$ are separated by the 3+/2+ wave. In addition to the nature of the redox events, the spacing of the waves in **1** is different compared to complexes **2**–**5**. The redox events for **1** begin at more positive potentials and are more widely spaced in relation to each other than those for **2**–**5**. The more positive potentials are likely due to the Cr center being trivalent instead of divalent, which would also affect the spacing between reduction waves.

DISCUSSION

The tripodal iminopyridine ligand $\mathbf{L}^{5\text{-OOMe}}$ displays considerable geometric flexibility in ligating first row transition-metal ions (Figure 1). Despite the structural diversity, when comparing the behavior of first row metal complexes **1**–**7**, the absorption spectra, electrochemical behavior, and many of the structural characteristics of this family of complexes are similar, and reflect the dominance of the ligand in determining physical properties. Below, we discuss in more detail some instances where significant metal–ligand interactions arise, including ligand field parameters relevant to spin-crossover applications, as well as the very different behavior of the Cr-containing compound **1** relative to the other species.

Electronic Structure Considerations for the "Cr(II)" Complex. Comparison of **1** and the one electron oxidized

dx.doi.org/10.1021/ic301909u | Inorg. Chem. 2012, 51, 12493–12502

counterpart $[Cr(\mathbf{L}^{5\text{-OOMe}})](BF_4)_3$[58] provides a more complete picture of the true electronic character of **1**. The cyclic voltammograms of the two Cr complexes are identical. The only difference in the electrochemical behavior between **1** and $[Cr(\mathbf{L}^{5\text{-OOMe}})](BF_4)_3$ is the rest potential of each complex and the nature of the event at most positive potential. In **1**, the most positive event is an oxidation and the rest potential lies between the first and second redox processes. In $[Cr(\mathbf{L}^{5\text{-OOMe}})](BF_4)_3$, the most positive event is a reduction and the rest potential lies positive of it.

Structurally, the two complexes are similar; however, several key distances in the iminopyridine ligand are different. Shown in Table 2, the lengthening of the C−N bond on the imine (z) and to a lesser extent on the pyridine (x), coupled with shortening of the C−C iminopyridine bridge (y) upon reduction from $[Cr(\mathbf{L}^{5\text{-OOMe}})]^{3+}$ to $[Cr(\mathbf{L}^{5\text{-OOMe}})]^{2+}$ is a hallmark of localization of the reducing equivalent on one arm of the iminopyridine ligand.[9] Comparison of the iminopyridine ligand bond lengths in **1** shows that one x and z in **1** are significantly longer than analogous average bond lengths in the other structurally characterized divalent complexes (also Table 2). Similarly, the one y in **1** is significantly shorter than its counterpart average in **2**−**5** and **7**. Along with the changes in ligand bond lengths, numerous intense bands in the absorption spectrum of **1**, including bands in the near IR, are features common to other complexes in which Cr(III) is bound by ligand radical anion species.[50]

Unrestricted B3LYP hybrid density functional results are consistent with the structural and spectroscopic studies. A comparison of **1** and $[Cr(\mathbf{L}^{5\text{-OOMe}})](BF_4)_3$ show that spin density on the metal center and first coordination sphere are nearly identical; in the divalent species (**1**), significant spin density is located in the π system of a single arm of the ligand $\mathbf{L}^{5\text{-OOMe}}$, as shown in Figure 4.

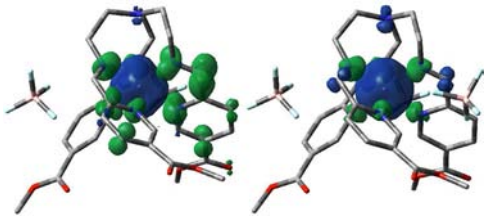

Figure 4. Net spin density plots for **1** (left) and $[Cr(\mathbf{L}^{5\text{-OOMe}})](BF_4)_3$ (right), scaled at 0.003 atomic units. Triplet and quartet states, respectively, are displayed. Blue surfaces correspond to net α spin density and green to net β spin density. Note additional β spin density on one pyridine "arm" of the iminopyridine ligand in the "Cr(II)" complex.

The M_S = 1 spin density plot for **1** can be characterized as a Cr(III) ($S = {}^3/_2$) ion antiferromagnetically coupled to a ligand-based electron. Comparison of low energy transitions (λ > 550 nm) for **1** and the anion of the free ligand support this model (Figures S3 and S4, Supporting Information). The magnetic moment indicating S = 1 is also consistent with strong antiferromagnetic coupling. All of these data point to the true identity of **1** as being $[Cr^{III}(\mathbf{L}^{5\text{-OOMe}})^-](BF_4)_2$.

Trends in Electronic Transitions for $\mathbf{L}^{5\text{-OOMe}}$ Complexes. Good qualitative agreement between experimental and TD-DFT-computed absorption spectra allow us to establish the orbital character of key features (via NTO analyses), important for the application of these kinds of complexes in solar photoconversion schemes. First, the importance of the bridgehead nitrogen atom is evident in the spectrum of the free ligand: all transitions involve the amine as a starting point. In turn, it is reasonable to expect that tuning the N···M distance in transition metal complexes will strongly perturb photophysical properties.

Second, it is evident that, for most of the first row complexes studied, the ligand dominates the transitions in the visible spectrum. The lowest energy transitions for **1** (Cr), **2** (Mn), **4** (Co), and **7** (Zn) show predominantly LLCT character, although it should be noted that the near-IR absorptions for **1** are related to a reduced ligand and are qualitatively different from the other compounds. Transitions featuring larger metal orbital contributions occur higher in energy, although with some overlap in the visible spectrum. The low-spin Fe(II) complex **3** is a clear exception, as its lowest energy transitions are largely MLCT in character. The lowest energy transition for the Ni(II) complex **5** is ligand field, as expected. A LMCT transition for the Cu(II) analogue **6** is predicted but not observed, at least not at the sample concentrations used. Overall, the $\mathbf{L}^{5\text{-OOMe}}$ ligand shows interesting potential for photophysical exploitation, provided that increased metal participation can be achieved. Compound **1** indicates that use of trivalent metals is promising; substituent tuning may offer an alternative route to increasing M−L interactions.

Electronic Structure Considerations for Spin-State Switching. For metals with d^4 to d^7 electron configurations in locally octahedral coordination environments, two spin states with different numbers of unpaired elections are possible, depending on whether electrons preferentially populate the e_g orbitals before filling the t_{2g} orbitals. The two energetic terms that dictate whether a complex has a high-spin (where S is maximized) or a low-spin (where S is minimized) configuration are the pairing energy, Π, required to pair electrons in the t_{2g} orbitals and the energy difference between the e_g and the t_{2g} orbitals, Δ_o.[59]

As discussed, the "Cr(II)" complex in **1** is better described as an antiferromagnetically coupled d^3 ligand radical anion system, and the high spin state is not accessible due to the strength of the coupling between the metal and ligand spin centers. Additionally, the ligand sets that have formerly demonstrated spin switching in Cr(II) and Mn(II) complexes do not include diimines or iminopyridines.[60] Spin switching has been observed for the d^4 $[Cr(depe)_2I_2]$,[61,62] where depe is 1,2-bis-(diethylphosphino)ethane, and for methyl and ethyl mono-alkylated Mn(II) manganocenes and the parent unfunctionalized compound, which all have d^5 configuration. Therefore, it is unsurprising that **1** remains S = 1 and **2** remains S = 5/2 down to the lowest temperatures probed (5 K). For the ligand system discussed here, we will only focus on the d^6 and d^7 species.

In d^6 Fe(II) complexes, iminopyridine ligands provide strong enough ligand fields[63,64] that unless functional groups ortho to the pyridine N are installed to sterically stabilize the high-spin state, the complexes are exclusively low spin at room temperature. We hypothesized that an electron withdrawing group at the 5-position may reduce the ligand field strength of the iminopyridine by pulling electron density away from the pyridine N, making it a weaker σ donor, and thus allow access to the spin-switching regime. The value of Δ_o (also, $10D_q$) calculated from the Ni(II) spectrum can be used to predict spin-crossover tendency in Fe(II) complexes using the same ligand set. For Ni(II) D_q values between 1120 and 1240 cm^{-1}, the corresponding Fe(II) complexes are expected to fall in the

dx.doi.org/10.1021/ic301909u | Inorg. Chem. 2012, 51, 12493−12502

spin-crossover range.[63,65] Therefore, based on the Ni(II) ligand field parameter alone, which is 0.1*Δ_o or 1155 cm^{-1}, this Fe(II) complex would be expected to exhibit spin-crossover. In this work, the available solution and solid state data indicate that the Fe(II) complex **3** remains low-spin at all conditions tested, signifying that the ester incorporation does not sufficiently weaken the ligand field for spin-crossover to manifest. We note that the ligand field parameters discussed above are merely guides for evaluating spin-crossover behavior with N_6 coordination environments, and that there are many exceptions which do not follow this trend. In this case, there may be geometric constraints introduced by tethering the three arms of the ligand together that preclude spin-crossover, which are not present in more commonly studied tris(diimine) Fe(II) complexes.[66]

For Co(II), strong ligand fields are necessary to force spin pairing in the d^7 species.[67] Previously, a $[Co(iminopyridine)_3]^{2+}$ complex had been reported as high-spin at room temperature, with gradual spin-crossover starting at approximately 250 K.[68] In the case of the tripodal ligand $L^{5\text{-}OOMe}$, while the magnetic moment for **4** does decrease as the temperature is lowered, it ultimately remains high spin in the solid state down to 5 K with a μ_{eff} of 4.15 μ_B. For an $S = 3/2$ ion and $g = 2$, the spin only μ_{eff} is expected to be 3.87 μ_B; the actual μ_{eff} for Co(II) species is frequently greater than this due to unquenched orbital angular momentum and g values are greater than 2. The stability of the high-spin state could be due to the weakened ligand field provided by the ester functionalized ligand, or it could be due to geometric constraints imposed by the tren capping group, which prevent reaching the low spin state. Notably, the hexadentate ligand may not allow for the exploitation of Jahn–Teller distortions common to bis-tridentate Co(II) complexes shown to be spin-crossover species, such as $[Co(terpy)_2]^{2+}$.[67,69] In those systems, stronger π-interaction occurs between the center N donor moieties on each of the ligands in comparison to the two flanking N donor moieties on each ligand. This effectively allows tetragonal compression along the z-axis, which favors the low-spin state over the high-spin state in Co(II) (less population of antibonding orbitals). Since there cannot be preferential imine versus pyridine coordination along the z-axis with $L^{5\text{-}OOMe}$, the Jahn–Teller-induced distortions observed in **4a** tend to be C_3 symmetric rather than tetragonal, and the low-spin state is not stabilized in **4** and **4a** even though the ligand field is strong enough to prevent access of the high-spin state in the Fe(II) analogue **3**.

CONCLUSIONS AND OUTLOOK

The survey of ester-functionalized iminopyridine complexes presented in this work display an interesting variety of coordination environments around the chelated metal ions. The complexes encompass geometries from very regular octahedral coordination, to highly strained trigonal antiprismatic, to seven-coordinate centers. Despite the wide variation in coordination, most of the complexes have very similar absorption spectra; they seem to divide into high-spin or low-spin electron configurations. Along with the absorption spectra, the electrochemical behaviors of the complexes are remarkably similar. These species display several ligand-based redox events that are mostly unperturbed by the metal identity. However, the redox state of the chelated metal dramatically affects these ligand-based redox events. In reality, the Cr complex **1** is best described as a Cr(III) metal center coordinated to a ligand radical anion, whereas complexes **2**–**7** are truly divalent metals chelated by a neutral ligand. Exploitation of ligand non-innocence in solar and/or thermal chemical transformations is underway. Additionally, ligand field considerations suggest that the Fe(II) analogue **3** is poised to display spin-crossover; however, **3** remains low-spin even at elevated temperatures. Exploring the role of ligand geometric constraints on spin-crossover accessibility will be pursued in due course.

ASSOCIATED CONTENT

Supporting Information

Additional tables and figures. CIF file of data. This material is available free of charge via the Internet at http://pubs.acs.org.

AUTHOR INFORMATION

Corresponding Author

*E-mail: matthew.shores@colostate.edu.

Notes

The authors declare no competing financial interest.

ACKNOWLEDGMENTS

This research was supported by the National Science Foundation (CHE-1058889), the Center for Revolutionary Solar Photoconversion, and Colorado State University. We thank Prof. O. P. Anderson and Dr. B. S. Newell for helpful discussions on X-ray crystallography.

REFERENCES

(1) Hoselton, M. A.; Wilson, L. J.; Drago, R. S. *J. Am. Chem. Soc.* **1975**, *97*, 1722–1729.
(2) Seredyuk, M.; Gaspar, A. B.; Ksenofontov, V.; Galyametdinov, Y.; Kusz, J.; Gütlich, P. *Adv. Funct. Mater.* **2008**, *18*, 2089–2101.
(3) Bowman, A. C.; Milsmann, C.; Bill, E.; Turner, Z. R.; Lobkovsky, E.; DeBeer, S.; Wieghardt, K.; Chirik, P. J. *J. Am. Chem. Soc.* **2011**, *133*, 17353–17369.
(4) Chen, Y.; Qian, C.; Sun, J. *Organometallics* **2003**, *22*, 1231–1236.
(5) Bianchini, C.; Mantovani, G.; Meli, A.; Migliacci, F.; Laschi, F. *Organometallics* **2003**, *22*, 2545–2547.
(6) Tang, X.; Sun, W.-H.; Gao, T.; Hou, J.; Chen, J.; Chen, W. *J. Organomet. Chem.* **2005**, *690*, 1570–1580.
(7) Vidyaratne, I.; Scott, J.; Gambarotta, S.; Budzelaar, P. H. M. *Inorg. Chem.* **2007**, *46*, 7040–7049.
(8) Stubbert, B. D.; Peters, J. C.; Gray, H. B. *J. Am. Chem. Soc.* **2011**, *133*, 18070–18073.
(9) Lu, C. C.; Bill, E.; Weyhermüller, T.; Bothe, E.; Wieghardt, K. *J. Am. Chem. Soc.* **2008**, *130*, 3181–3197.
(10) Ni, Z.; McDaniel, A. M.; Shores, M. P. *Chem. Sci.* **2010**, *1*, 615–621.
(11) McDaniel, A. M.; Tseng, H.-W.; Damrauer, N. H.; Shores, M. P. *Inorg. Chem.* **2010**, *49*, 7981–7991.
(12) Larsen, E.; LaMar, G. N.; Wagner, B. E.; Parks, J. E.; Holm, R. H. *Inorg. Chem.* **1972**, *11*, 2652–2668.
(13) McLachlan, G. A.; Fallon, G. D.; Spiccia, L. *Acta Crystallogr., Sect. C: Cryst. Struct. Commun.* **1996**, *52*, 309–312.
(14) Qian, M.; Gou, S. H.; He, L.; Zhou, Y. M.; Duan, C. Y. *Acta Crystallogr., Sect. C: Cryst. Struct. Commun.* **1999**, *55*, 742–744.
(15) Li, S.-N.; Ren, Y.-W.; Li, J.; Zhang, F.-X.; Hu, M.-C. *Acta Crystallogr., Sect. E: Struct. Rep. Online* **2006**, *62*, m498–m499.
(16) Kirchner, R. M.; Mealli, C.; Bailey, M.; Howe, N.; Torre, L. P.; Wilson, L. J.; Andrews, L. C.; Rose, N. J.; Lingafelter, E. C. *Coord. Chem. Rev.* **1987**, *77*, 89–163.
(17) Gütlich, P.; Hauser, A. *Coord. Chem. Rev.* **1990**, *97*, 1–22.
(18) Gütlich, P.; Garcia, Y.; Goodwin, H. A. *Chem. Soc. Rev.* **2000**, *29*, 419–427.
(19) Halcrow, M. A. *Chem. Soc. Rev.* **2011**, *40*, 4119–4142.
(20) Halcrow, M. A. *Polyhedron* **2007**, *26*, 3523–3576.

(21) Klug, C. M.; McDaniel, A. M.; Fiedler, S. R.; Schulte, K. A.; Newell, B. S.; Shores, M. P. *Dalton Trans.* **2012**, *41*, 12577−12585.
(22) Toftlund, H. *Coord. Chem. Rev.* **1989**, *94*, 67−108.
(23) We note that cyclic imines other than pyridine have been condensed with tren to generate multidentate tripodal ligands.[19,20] However, for this work, our focus is on iminopyridine species.
(24) Seredyuk, M.; Gaspar, A. B.; Ksenofontov, V.; Galyametdinov, Y.; Kusz, J.; Gütlich, P. *J. Am. Chem. Soc.* **2008**, *130*, 1431−1439.
(25) Seredyuk, M. *Inorg. Chim. Acta* **2012**, *380*, 65−71.
(26) Qu, P.; Meyer, G. J. *Langmuir* **2001**, 6720−6728.
(27) Ni, Z.; Shores, M. P. *J. Am. Chem. Soc.* **2008**, *131*, 32−33.
(28) Oila, M. J.; Tois, J. E.; Koskinen, A. M. P. *Tetrahedron Lett.* **2005**, *46*, 967−969.
(29) Jabre, N. D.; Respondek, T.; Ulku, S. A.; Korostelova, N.; Kodanko, J. J. *J. Org. Chem.* **2010**, *75*, 650−659.
(30) Henriques, R. T.; Herdtweck, E.; Kuhn, F. E.; Lopes, A. D.; Mink, J.; Romao, C. C. *J. Chem. Soc., Dalton Trans.* **1998**, 1293−1297.
(31) Hagen, K. S. *Inorg. Chem.* **2000**, *39*, 5867−5869.
(32) Shavaleev, N. M.; Scopelliti, R.; Gumy, F.; Bünzli, J.-C. G. *Inorg. Chem.* **2009**, *48*, 6178−6191.
(33) *APEX 2*; Bruker Analytical X-Ray Systems, Inc.: Madison, WI, 2008.
(34) Sheldrick, G. M. *SHELXTL*, Version 6.14; Bruker Analytical X-Ray Systems, Inc.: Madison, WI, 1999.
(35) Spek, A. L. *J. Appl. Crystallogr.* **2003**, *36*, 7−13.
(36) Bain, G. A.; Berry, J. F. *J. Chem. Educ.* **2008**, *85*, 532−536.
(37) Evans, D. F. *J. Chem. Soc.* **1959**, 2003−2005.
(38) Live, D. H.; Chan, S. I. *Anal. Chem.* **1970**, *42*, 791−792.
(39) Ostfeld, D.; Cohen, I. A. *J. Chem. Educ.* **1972**, *49*, 829.
(40) Schubert, E. M. *J. Chem. Educ.* **1992**, *69*, 62.
(41) Grant, D. H. *J. Chem. Educ.* **1995**, *72*, 39.
(42) Becke, A. D. *J. Chem. Phys.* **1993**, *98*, 5648−5652.
(43) Frisch, M. J.; et al. *Gaussian 03*; Gaussian, Inc.: Wallingford, CT, 2004.
(44) Hay, P. J.; Wadt, W. R. *J. Chem. Phys.* **1985**, *82*, 299−310.
(45) Ditchfield, R.; Hehre, W. J.; Pople, J. A. *J. Chem. Phys.* **1971**, *54*, 724−728.
(46) Hehre, W. J.; Ditchfield, R.; Pople, J. A. *J. Chem. Phys.* **1972**, *56*, 2257−2261.
(47) Binkley, J. S.; Pople, J. A.; Hehre, W. J. *J. Am. Chem. Soc.* **1980**, *102*, 939−947.
(48) Francl, M. M.; Pietro, W. J.; Hehre, W. J.; Binkley, J. S.; Gordon, M. S.; DeFrees, D. J.; Pople, J. A. *J. Chem. Phys.* **1982**, *77*, 3654−3665.
(49) Herzog, S.; Aul, H. *Z. Naturforsch.* **1960**, *15b*, 617.
(50) Scarborough, C. C.; Sproules, S.; Weyhermüller, T.; DeBeer, S.; Wieghardt, K. *Inorg. Chem.* **2011**, *50*, 12446−12462.
(51) The trigonal pocket side lengths were taken as the distances between the oxygen atoms in each ester group which faced toward the meal center. In all cases except the Fe(II) complex **3**, this was the noncarbonyl oxygen atom of each ester.
(52) Chum, H. L.; Rock, M.; Murakami, N. Y.; Jordan, I.; Rabockai, T. *J. Electroanal. Chem.* **1977**, *76*, 277−285.
(53) Choudhury, S.; Deb, A. K.; Goswami, S. *Polyhedron* **1994**, *13*, 1062−1068.
(54) Da Luz, D.; Franco, C. V.; Vencato, I.; Neves, A.; Mascarenhas, Y. P. *J. Coord. Chem.* **1992**, *26*, 269−283.
(55) Kryatov, S. V.; Mohanraj, B. S.; Tarasov, V. V.; Kryatova, O. P.; Rybak-Akimova, E. V.; Nuthakki, B.; Rusling, J. F.; Staples, R. J.; Nazarenko, A. Y. *Inorg. Chem.* **2002**, *41*, 923−930.
(56) Marrs, D. J.; McKee, V.; Nelson, J.; Lu, Q.; Harding, C. J. *Inorg. Chim. Acta* **1993**, *211*, 195−202.
(57) Qin, L.; Nelson, J.; McCann, M. *J. Inorg. Biochem.* **1993**, *51*, 633−639.
(58) McDaniel, A. M.; Tseng, H.-W.; Hill, E. A.; Damrauer, N. H.; Rappé, A. K.; Shores, M. P., submitted.
(59) Hauser, A. *Top. Curr. Chem.* **2004**, *233*, 49−58.
(60) Garcia, Y.; Gütlich, P. *Top. Curr. Chem.* **2004**, *234*, 786.
(61) Halepoto, D. M.; Holt, D. G. L.; Larkworthy, L. F.; Leigh, G. J.; Povey, D. C.; Smith, G. W. *J. Chem. Soc., Chem. Commun.* **1989**, 1322−1323.
(62) Halepoto, D. M.; Holt, D. G. L.; Larkworthy, L. F.; Povey, D. C.; Smith, G. W.; Leigh, G. J. *Polyhedron* **1989**, *8*, 1821−1822.
(63) Goodwin, H. A. *Top. Curr. Chem.* **2004**, *233*, 59−90.
(64) Toftlund, H.; McGarvey, J. J. *Top. Curr. Chem.* **2004**, *233*, 151−166.
(65) Robinson, M. A.; Curry, J. D.; Busch, D. H. *Inorg. Chem.* **1963**, *2*, 1178−1181.
(66) We note that the apparent ligand field parameter is actually stronger for the ester-containing ligand $\mathbf{L}^{5\text{-OOMe}}$ (1155 cm^{-1}) as compared to its counterpart without ester functionalization (1124 cm^{-1}).[65] This is unexpected, since the addition of an electron withdrawing group is expected to decrease σ donation ability and provide a weaker ligand field. We also note that there is a scaling factor (between 1.1 and 1.0)[65] for converting between the Ni(II) ligand field to the Fe(II) ligand field that could account for the discrepancy in the apparent ligand field parameters vs the nature of the ligand functional groups.
(67) Goodwin, H. A. *Top. Curr. Chem.* **2004**, *234*, 786.
(68) Mueller, E. W.; Spiering, H.; Gütlich, P. *Inorg. Chem.* **1984**, *23*, 119−120.
(69) Figgins, P. E.; Busch, D. H. *J. Phys. Chem.* **1961**, *65*, 2236−2240.